Boletín de la Sociedad Española de Cerámica y Vidrio
Vol 50, 3, 135-142, Mayo-Junio 2011 ISSN 0366-3175. eISSN 2173-0431.
doi: 10.3989/cyv.182011

BOLETIN DE LA SOCIEDAD ESPAÑOLA DE
Cerámica y Vidrio
A R T I C U L O

Ni-YSZ Substrate Degradation during Carbon Deposition

MARJAN MARINŠEK

University of Ljubljana, Faculty of Chemistry and Chemical Technology, Aškerčeva 5, 1000 Ljubljana, Slovenia
marjan.marinsek@fkkt.uni-lj.si Tel.: +386 1 2419 204 Fax: +386 1 2419 220

Carbon deposition on various Ni-YSZ catalytic composites with average Ni particle size from 0.44 μm to 0.98 μm was studied under dry CH_4-Ar and humidified CH_4-Ar conditions. The change in the catalytic activity was monitored both as a mass gain due to carbon deposition and hydrogen evolution due to CH_4 dehydrogenation on Ni-YSZ. Regarding the start of methane decomposition and subsequent catalyst deactivation rate, composites with smaller Ni-grains were much more active in comparison to those with relatively large grains. Dry methane conditions always caused coking of the catalyst substrate with substantial activity loss. In contrast, under humidified methane atmosphere conditions with a steam to carbon (S/C) ratio of 0.82, catalytic activity of the Ni-YSZ composites remained nearly undiminished after 2,000 minutes at chosen deposition temperatures (600–800 °C). On the catalyst surface, some encapsulation of Ni with the deposited carbon was noticed while carbon filaments grew inside the treated samples. The dimensions of C-filaments were influenced by treatment conditions and Ni-YSZ substrate morphology.

Key words: Fuel cells, Carbon deposition, Microstructure, Microscopy

Ni-YSZ Degradación de substrato durante la deposición de carbón

La deposición de carbón en diferentes compuestos catalizadores Ni-YSZ con un tamaño promedio de partícula Ni de 0.44 μm a 0.98 μm fue estudiado bajo condiciones secas: CH_4-Ar y húmedas: CH_4-Ar. El cambio de la actividad catalítica fue monitoreado tanto como una ganancia de masa debida a la deposición de carbón y una evolución de hidrógeno debido a la deshidrogenación de CH_4 en Ni-YSZ. En cuanto al comienzo de descomposición del metano y a la subsiguiente desactivación del catalizador, aquellos compuestos con granos Ni menores fueron mucho más activos en comparación a aquellos con granos relativamente mayores. Las condiciones secas del metano siempre causaron coquificación del sustrato del catalizador con una sustancial pérdida de actividad. Por el contrario, en el metano bajo una atmósfera húmeda con un ratio S/C de 0.82, la actividad catalizadora de los compuestos Ni-YSZ permaneció prácticamente sin disminuciones luego de 2,000 minutos bajo las temperaturas de deposición seleccionadas (600–800 °C). En la superficie de catalización se observó cierta encapsulación de Ni con el carbón depositado, mientras que los filamentos de carbón se desarrollaron dentro de las pruebas tratadas. Las dimensiones de los filamentos C fueron influenciados por las condiciones del tratamiento y la morfología del sustrato Ni-YSZ.

Palabras clave: Células de combustible, Deposición de carbón, Microestructura, Microscopía

1. INTRODUCTION

Solid oxide fuel cells (SOFCs) are one of the most attractive energy conversion systems because of their high efficiency, low pollution and multi-fuel compatibility. The high operating temperature gives rise to excellent fuel flexibility, allowing also hydrocarbons to be fed directly to the anode site of an SOFC module [1-5]. However, the use of hydrocarbons as fuel is often accompanied by two major problems: the risk of carbon deposition covering the active catalyst sites, subsequently resulting in the catalyst deactivation, loss of cell performance and lower SOFC reliability [6, 7], and the creation of severe temperature gradients due to the significant cooling effect of the hydrocarbon reforming process, which may eventually lead to the material physical degradation.

Many reports describing the use of hydrocarbons as SOFC fuel, either for their direct oxidation or in their internal reforming, revealed that relatively low carbon deposition rates are expected if SOFC anodes are based on copper[8, 9], doped ceria [10, 11], or other conducting oxides [12, 13]. Unfortunately, the performance of these anodes tends to be in some respects poor compared to Ni-based anodes, because Cu is inferior to Ni as an electrocatalyst, and oxides have lower electronic conductivities then metals. Therefore, Ni-based anodes still appear to be attractive candidates for SOFCs if the problem of carbon formation and its consequence can be overcome.

The majority of studies, both experimental and theoretical, on Ni-YSZ-based cermet anodes devoted to the minimization of carbon deposition have focused on the steam-to-carbon ratio (S/C) in the anode supply gas, effective inhibitors for carbon deposition, and appropriate Ni-YSZ microstructure [14-16]. It was reported that dry methane or a methane-steam anode gaseous mixture with an insufficient steam addition would lead to methane

cracking, yielding carbon deposits on the catalyst surface [16-20]. The cracking reaction is even more problematic with higher hydrocarbons, which are also present in natural gas. Therefore an S/C ratio >2 is required for minimum problems of carbon formation. Some additives like MgO, CaO, SrO and CeO_2 or Ru and Pt to Ni-YSZ cermet may also be effective in promoting steam reforming of CH_4 and suppressing carbon deposition [21-26].

Thermodynamic calculations are often used to predict conditions in which carbon formation can be avoided. For example, with methane as the fuel, thermodynamic calculations suggest that carbon should not form at 1073 K and $P_{tot.}$ = 1 atm with an S/C ratio greater than one [27]. However, experimentally Ni will promote carbon formation under these conditions, as well as other conditions in which carbon formation is not thermodynamically predicted [28, 29]. Such experimental work indicates that carbon deposition (coking) on active catalyst sites is not a simple process. It involves several reaction steps that may eventually lead to various CH_x species formation on the catalyst surface, which are finally decomposed into carbon and hydrogen [30, 31].

Carbon formation on Ni catalysts has been studied for many years [17, 32, 33]. It was proposed that several types of carbon, including absorbed, polymeric, vermicular filaments, carbide, and graphitic carbon can form on supported Ni catalyst. The type of carbon deposited depends on the temperature of formation and specific reactants i.e. CO versus hydrocarbons. It should be emphasized that some forms of deposited carbon result in loss of catalytic activity (i.e. encapsulation of metal surface with graphitic carbon) while others have greater influence on the mechanical stability of the catalyst (i.e. growth of carbon filaments, fibers or whiskers).

The aim of this work was to illustrate the degradation process of Ni-YSZ cermets due to catalytic decomposition of CH_4 and subsequent carbon deposition. For this purpose, Ni-YSZ cermets with various microstructures were prepared and exposed to dry or humidified methane at different temperatures. Carbon deposition process was studied under non-electrochemical conditions (zero-voltage conditions) where self de-coking (reaction of deposited carbon with oxygen ions supplemented from the lattice of an oxygen-ion conductor) did not take place. Such a configuration enables experimental work solely on the anode layer without the need of constructing the whole SOFC. Non-electrochemical circumstances are probably also the most likely conditions for carbon formation in an operating SOFC.

2. EXPERIMENTAL PROCEDURE

2.1. Ni-YSZ cermet preparation:

NiO-YSZ composite powders were prepared with a modified combustion synthesis. The combustion system was based on the citrate/nitrate redox reaction [34,35]. In this combustion method, the staring materials were $ZrO(NO_3)_2{\cdot}6H_2O$, $Ni(NO_3)_2{\cdot}6H_2O$, $Y(NO_3)_3{\cdot}6H_2O$, nitric acid (65 %), and citric acid (analytical reagent grade). All solid compounds were dissolved with minimum additions of water in the amounts that assure the desired Ni content in final cermet (50 vol.% Ni). $ZrO(NO_3)_2{\cdot}6H_2O$ and $Y(NO_3)_3{\cdot}6H_2O$ additions were calculated to assure final YSZ composition to be $Zr_{0,85}Y_{0,15}O_{1,93}$. The five reactant solutions were mixed together to prepare the reaction mixture and then treated under vacuum (20 mm Hg,) at 60 °C until the solution transformed into a bright green gel. Typical amounts of precursors used in one batch were 4.764 g $ZrO(NO_3)_2{\cdot}6H_2O$, 14.989 g $Ni(NO_3)_2{\cdot}6H_2O$, 0.936 g $Y(NO_3)_3{\cdot}6H_2O$, 7.369 g $C_6H_8O_7{\cdot}H_2O$, and 4 mL HNO_3. The gel was then gently milled in an agate mortar and uni-axially pressed (17 MPa) into pellets (ϕ = 12 mm, height ~30 mm). These samples were placed on a corundum plate and ignited at the top of the pellet. High temperatures were reached in a short reaction time by self-generated heat of reaction, yielding nanopowders or loose agglomerates of nanocrystallites. The grain size of both phases in the synthesized composite material (prior attritor milling) was investigated by TEM (JEM-2010F TEM/STEM, operated at 200 keV, equipped with an URP pole-piece (C_S = 0.48 mm), EDS and PEELS). The powders for TEM microscopy were gently crushed in an agate mortar. A dilute suspension was prepared in absolute alcohol. A drop of the suspension was deposited on a holey carbon-coated copper grid, which was subsequently dried. In the TEM mode, both bright-field (BF) and dark-field (DF) images were recorded with the corresponding electron diffraction patterns (SAED). According to TEM investigations, such synthesized particles are a random mixture of NiO and YSZ. Indexing of the diffraction rings shows that both phases are crystalline. The measured average crystallite size estimated from the HRTEM image for the two phases was 6.5±2 nm. Such a oxide mixture was the starting material for the final Ni-YSZ cermet preparation.

After the synthesis, the powders were milled in attritor mill (4 hours). Milled samples were then used for green body preparation (uni-axially pressed into pellets ϕ = 8 mm

TABLE 1. QUANTITATIVE MICROSTRUCTURE ANALYSIS OF THE REDUCED SAMPLES NI-YSZ

Sample	$T_{sintr.}$ / °C	ε / %		$\bar{d}$ / μm		
		geom.	micr.	Ni	YSZ	pores
A	1150	44.7	41.2	0.44	0.10	0.16
B	1200	30.1	29.9	0.27	0.17	0.19
C	1300	25.7	32.6	0.55	0.45	0.35
D	1400	25.2	28.5	0.98	0.70	0.96

Bol. Soc. Esp. Ceram. Vidr. Vol 50. 3, 135-142, mayo-junio 2011. ISSN 0366-3175. eISSN 2173-0431. doi: 10.3989/cyv.182011

with 100 MPa) and sintered at different temperatures (1150 °C, 1200 °C, 1300 °C, 1400 °C, heating rate 10 K/min, $t_{sintr.}$ = 1 h). For microstructure determination, sintered tablets were polished (diamond paste 3 and 0.25 μm), thermally etched, reduced (at 900 °C for 2 hours) in H_2/Ar atmosphere and subsequently analyzed with a SEM (Zeiss FE SUPRA 35 VP). Phase compositions of the samples were analyzed by EDS, supported by INCA software (Oxford Instruments). The quantitative analysis of the microstructures was performed on digital images (images were digitized into pixels with 255 different gray values using Zeiss KS300 3.0 image-analysis software). For statistically reliable data, in each case five to ten different regions were analyzed. The results of the quantitative microstructure analysis are summarized in Table 1 (porosity ε was determined both as geometrical from the size and mass of the sintered samples as well as from the microstructural analysis, while parameters $\bar{d}$ is represented as diameter of the area-analogue circle – DCIRCLE). Ni surface area investigation by H_2 selective adsorption was performed on sintered tablets using Micromeritics ASAP 2020 apparatus.

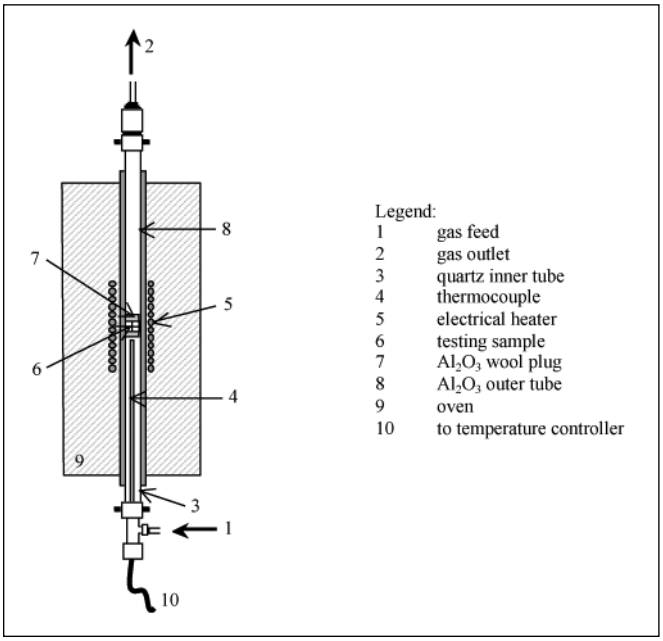

Figure 1. Configuration of the experimental set-up for carbon deposition tests.

2.2. Carbon deposition tests:

Carbon deposition tests were conducted in a tube oven (Figure 1). A sintered sample (NiO-YSZ tablet) was placed between two Al_2O_3 wool plugs in the middle of the inner tube (quartz) and placed into the oven. A full cycle of carbon deposition experiment always started with the sample reduction, where NiO-YSZ tabled was treated in an Ar-H_2 (5 vol. % H_2) atmosphere (heating rate 10 K/min) from room temperature up to 900 °C, followed by an isothermal treatment at 900 °C for two hours. After cooling the system down in Ar-H_2 atmosphere to a desired temperature of carbon deposition test (cooling rate 10 K/min), Ar-CH_4 (4 vol. %) or humidified Ar-CH_4 atmosphere was then fed to the catalyst bed at a total flow rate of 50 mL/min. The exact conditions of samples' treatment in methane involving atmosphere are summarized in Table 2. When a humidified Ar-CH_4 mixture was used for the carbon deposition tests, the S/C ratio was kept at 0.82, meaning that carbon deposition should have been thermodynamically avoided. The final sample cooling from the carbon deposition temperature back to room temperature was made in an Ar (5.0) atmosphere.

Separately, carbon deposition on Ni/YSZ substrate was followed also by mass change measurements (TG - Netzsch STA 409 apparatus) while an evolved gas analysis was used for the determination of the released hydrogen (EGA-Netzsch STA 409 coupled to a QMS Pfeiffer PrismaPlus 220). Deposition conditions including NiO-YSZ reduction were the same as in the case of the experiments in tube-oven.

TABLE 2. EXPERIMENTAL CONDITIONS DURING ISOTHERMAL DEPOSITION TESTS IN A TUBE-OVEN

Sample	$T_{sintr.}$ / °C	$T_{dep.}$ / °C	$t_{dep.}$ / h	atmosphere	Final sample description
A2	1150	600	40	CH_4	large surface cracks
B1	1200	500	120	CH_4	large surface cracks
B2	1200	600	40	CH_4	small surface cracks
B3	1200	700	20	CH_4	small surface cracks
B4	1200	800	7	CH_4	large surface cracks
C1	1300	500	120	CH_4	small surface cracks
C2	1300	600	40	CH_4	small surface cracks
D2	1400	600	40	CH_4	no visual surface changes
A'2	1150	600	96	$CH_4 + H_2O$	large surface cracks
B'1	1200	500	264	$CH_4 + H_2O$	small surface cracks
B'2	1200	600	96	$CH_4 + H_2O$	small surface cracks
B'3	1200	700	45	$CH_4 + H_2O$	no visual surface changes
B'4	1200	800	15	$CH_4 + H_2O$	no visual surface changes
C'1	1300	500	264	$CH_4 + H_2O$	no visual surface changes
C'2	1300	600	96	$CH_4 + H_2O$	no visual surface changes
D'2	1400	600	96	$CH_4 + H_2O$	no visual surface changes

3. RESULTS AND DISCUSSION

Quantitative microstructure analysis of the prepared Ni-YSZ cermets revealed that higher sintering temperatures resulted in pronounced grain growth of both phases. Exaggerated Ni-coarsening in the case of sample A was ascribed to the microstructure instability of the final Ni-YSZ cermet due to too low sintering temperature. Specifically, if the YSZ framework after sintering is not rigid enough, it cannot withstand the tendency of new formed Ni grains during the reduction to sinter. However, an average one-phase grain expressed as DCIRCLE remained in sub-micro meter range if the cermets had been sintered below 1400 °C (Table 1). The differences in Ni-grain morphology were reflected also during metallic surface area determination. Thus, Ni-surface area in sample A (sintered at 1150 °C) was measured as 1.2 m^2/g_{Ni}, while in sample D (sintered at 1400 °C) Ni-surface area diminished to 0.4 m^2/g_{Ni}.

These microstructure parameters are very important, since they directly influence the material activity for hydrocarbons conversion (as well as the anode electrochemical activity and long term stability in an operating cell). In general, from the activity point of view, the cermets composed of nano-sized grains are preferable to those whose one-phase dominance grains are relatively large. However, regarding hydrocarbon treatment inside the Ni-YSZ anode layers, very high initial conversion rates may cause also undesired carbon deposition, which eventually covers the active catalyst sites and may even physically damage the catalyst.

In the experimental work, the cermets activity was monitored both as a mass gain due to carbon deposition and hydrogen evolution. The monitored parameters are comparable, since any carbon deposition, as a consequence of methane dissociation, also produces hydrogen evolution. According to the results in Figures 2 and 3, there was a clear difference regarding mass gain or hydrogen evolution among samples. Composites with smaller Ni-grains were much more active compared to those with relatively large grains. Specifically, during early stages of the deposition tests, smaller Ni-grains started to catalyze methane decomposition at lower temperatures, as indicated by a sharp initial peak in hydrogen evolution curves (Figure 2 – dynamic test). Furthermore, during the isothermal tests, sample A (sintered at 1150 °C) deactivated more slowly in comparison to sample D (sintered at 1400 °C). In other words, at the beginning of the isothermal part, carbon in sample A deposited at a rate $r_{c_A}(t_0)$ $3.10 \cdot 10^{-3}$ $mg_{(C)} \cdot (g_{(cat)}s)^{-1}$. This value after 850 minutes slowly diminished to $r_{c_A}(t_{850})$ $1.44 \cdot 10^{-3}$ $mg_{(C)} \cdot (g_{(cat)}s)^{-1}$ and further remained fairly

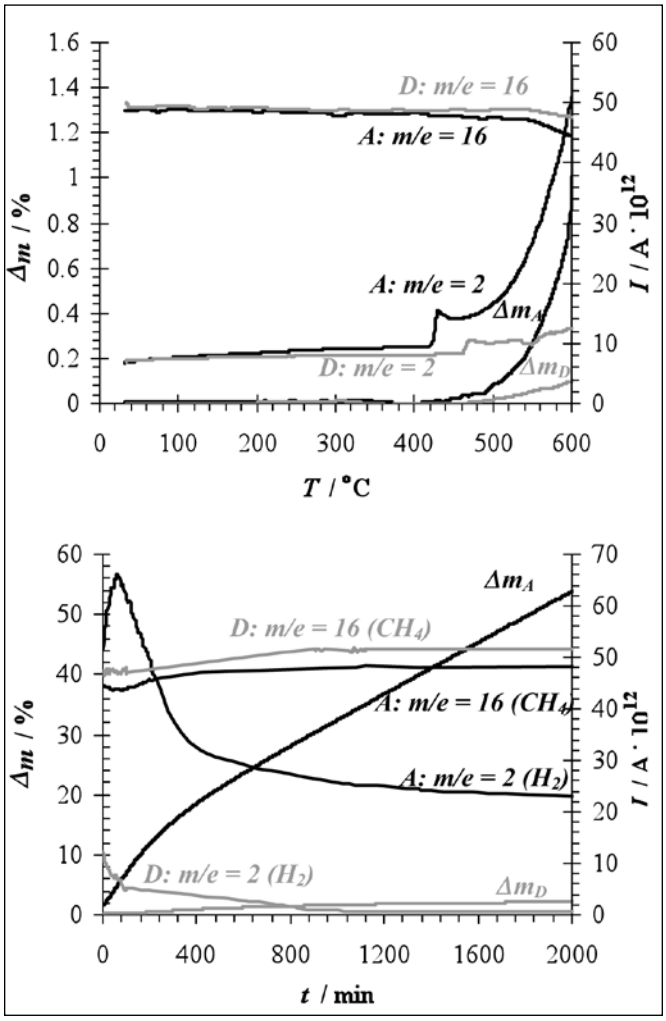

Figure 2. Carbon deposition in Ni-YSZ cermets with various microstructure characteristics taken in Ar-CH_4 atmosphere (dynamic test – left followed by an isothermal test – right)

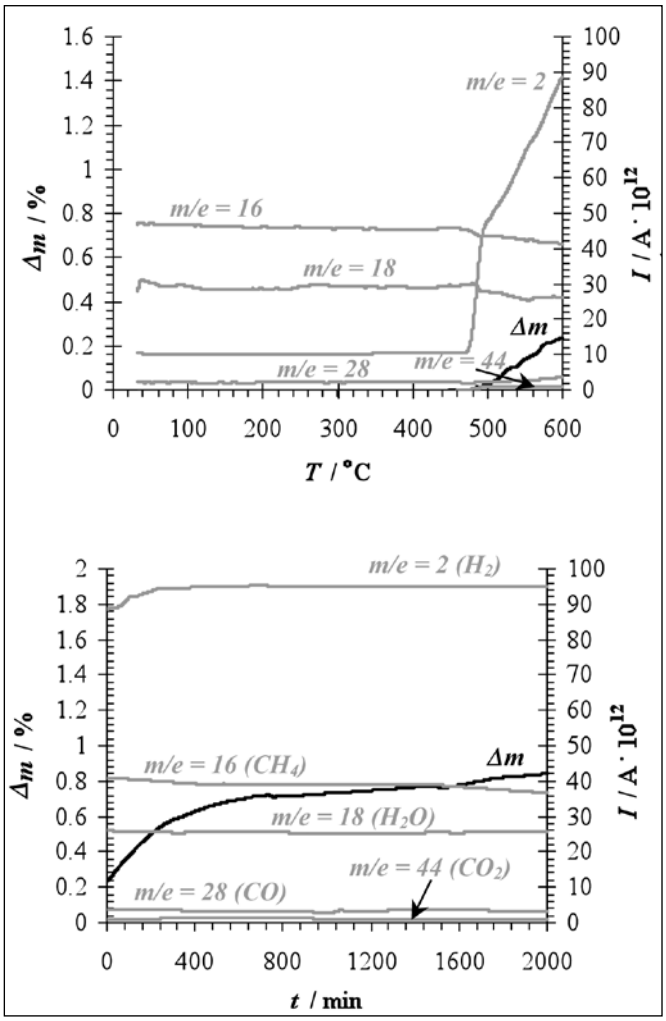

Figure 3. Carbon deposition in sample A taken in Ar-CH_4-H_2O atmosphere (dynamic test – left followed by an isothermal test – right)

Bol. Soc. Esp. Ceram. Vidr. Vol 50. 3, 135-142, mayo-junio 2011. ISSN 0366-3175. eISSN 2173-0431. doi: 10.3989/cyv.182011

constantly. In sample D, r_{C_D} (t_0) reached value $0.17 \cdot 10^{-3}$ $mg_{(C)} \cdot (g_{(cat)}s)^{-1}$, then further diminished and after 1200 minutes reached a rather constant and minimum value r_{C_D} (t_{1200}) $0.03 \cdot 10^{-3}$ $mg_{(C)} \cdot (g_{(cat)}s)^{-1}$. Expressed with the specific catalyst activity α defined as ,

$$\alpha = r_C(t) / r_C(t_0)$$

sample A at 600 °C retained 46.5% of its initial activity after reaching point of the constant carbon deposition rate, while sample D retained only 17.7% of the initial activity.

Carbon deposition and consequent hydrogen evolution may differ somewhat if gas fed to the reactor contains water (Figure 3). In this case, gases evolved during methane decomposition, except for hydrogen and unreacted methane, also contained H_2O, CO and CO_2 as a result of methane decomposition and equilibrium reactions between gaseous products. However, although mass gain in this later case was much smaller (0.84 % in 2,000 minutes) carbon was still depositing when CH_4-H_2O fed gas with S/C ratio 0.82 was used. Another distinctive fact among the tested samples is associated with their activity loss. Activity for the methane decomposition of samples treated in non-humidified methane atmosphere decreased relatively quickly after reaching the isothermal part of tests as shown with hydrogen evolution curves. In the extreme case of sample D, activity for methane decomposition after 2,000 minutes at 600°C was almost completely lost. In contrast, in the humidified methane atmosphere hydrogen evolution continued practically undiminished without any catalytic activity loss. This fact may imply that different catalyst surface poisoning mechanisms may be involved in both cases.

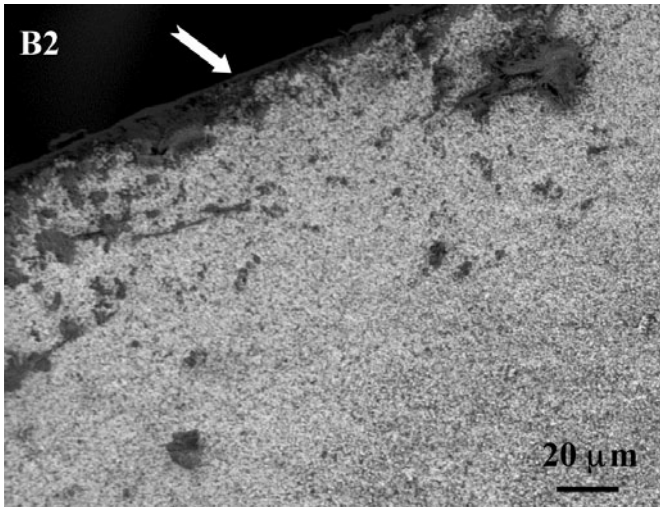

Figure 4. Cross section of sample B2 after carbon deposition $T_{dep.}$ = 600 °C $t_{dep.}$ = 40 h. Sample surface is almost completely covered with the deposited carbon (arrow on the left image) and formed cracks on the surface in sample B1 (right image)

Carbon deposition on Ni-YSZ catalyst in the methane-containing atmosphere was monitored into more detail with a microstructure investigation of the samples after treatment in the tube-oven. It was observed that Ni-YSZ cermet characteristics have great influence on the amount and form of the deposited carbon. Firstly, the appearance of

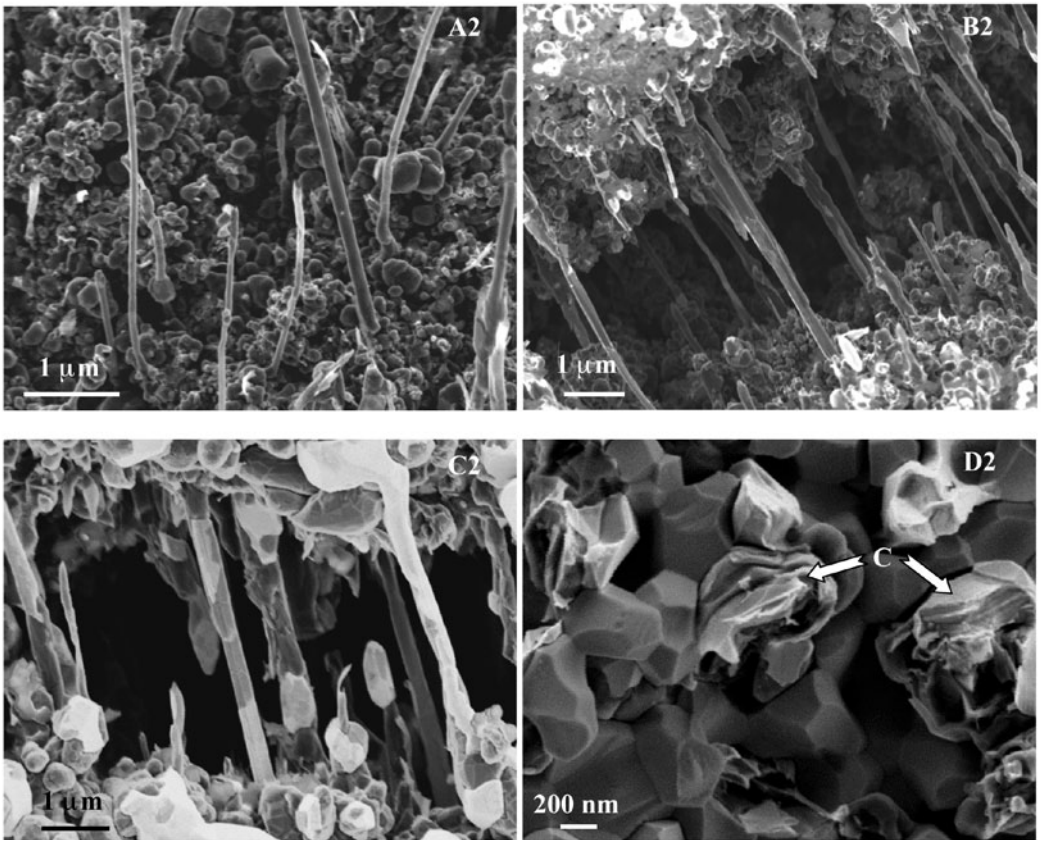

Figure 5. C-filament growth inside samples A2-C2 and encapsulation of Ni grains with the deposited carbon in sample D2 (note that magnification bar is not identical in all micrographs)

the deposited carbon may differ significantly at the surface or inside the exposed tablets. On the sample surface, prolonged treatment in the methane-containing atmosphere always caused some carbon deposition on Ni grains and in some extreme situations, like relatively long exposure times and a dry atmosphere, almost complete coverage of the surface with the deposited carbon (Figure 4).

In contrast, in many samples carbon filaments were found inside the treated pellets. The appearance and the dimensions of the grown filaments seemed to be very much dependent on the Ni morphological characteristics (Figure 5). In other words, if the pellets were sintered at lower temperatures (from 1150 °C to 1300 °C – samples A-C) then the final Ni grains remained small enough to promote carbon filaments growth. The diameter of the grown filaments increased with the size of Ni-grains. Such a phenomenon has already been described in the literature. Specifically, relatively small catalytic particles produce carbon nanofibers with smaller diameters while larger particles do not promote filament growth [36-38]. In contrast, treatment at 1400 °C caused excessive grain growth during sintering, which resulted in relatively large Ni grains (samples D) after the reduction. In the samples with such relatively large Ni grains ($\overline{d_{Ni}} \approx 1$ μm), the deposited carbon never grew as filaments, but rather as plates encapsulating Ni grains.

Beside catalyst morphology, deposition conditions also influence the dimensions of the grown C-filaments (Figure 6). Specifically, carbon filaments grew to larger diameters if the deposition temperature was higher. In contrast, lower deposition temperatures resulted in more uniform fibers with narrower diameters.

When humidified methane was used in the reaction chamber, the situation regarding the form of the deposited carbon was very similar; i.e. some Ni-grain encapsulation with carbon may be found on the sample surface and carbon filaments inside the treated samples (Figure 7). The main difference between wet methane- and dry methane-treated samples was in the time required before some physical degradation of the substrate was noticed. The time required for crack formation in the case of humidified methane-treated samples was substantially longer. Figure 7: Formed cracks on the A'2 sample surface …

One of the most interesting observations during the experimental work was the fact that irrespective of atmosphere used C-filaments always appeared inside the formed cracks. Furthermore, it seems that C-fiber growth is actually the cause for sample cracking and eventually in complete physical degradation of the substrate microstructure. In the case of A-C samples, the cracks formed grew with time as C-nanofibers appeared deeper inside the sample (Figure 8). In contrast, in the

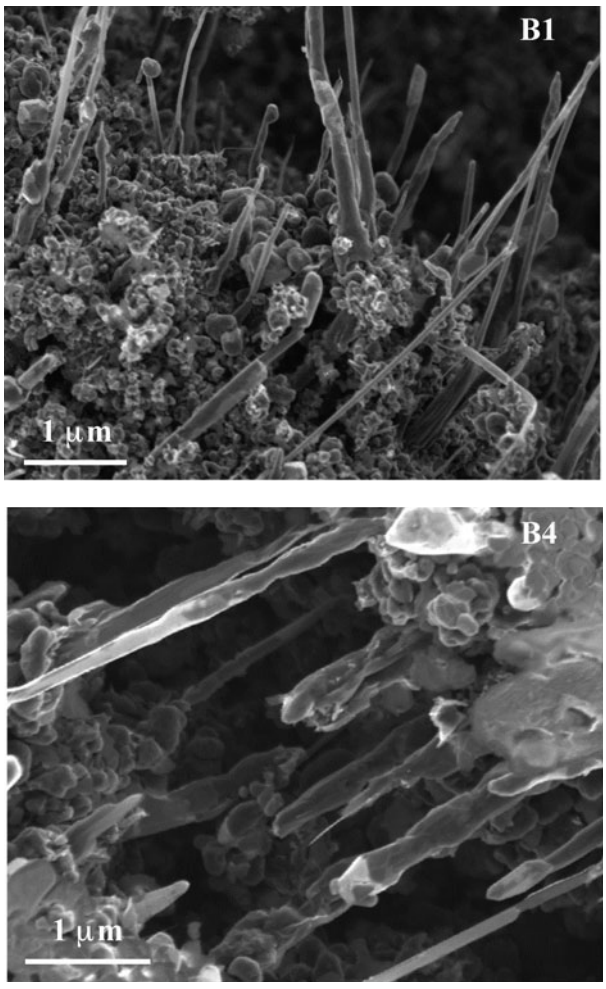

Figure 6. Dimensions of the grown C-nanotubes as a function of the deposition conditions

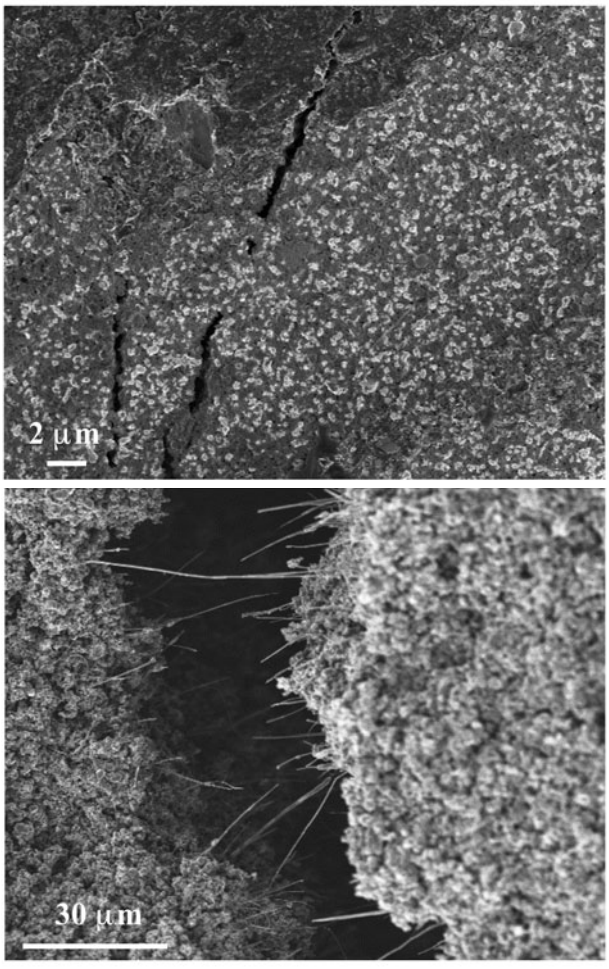

Figure 7. Formed cracks on the A'2 sample surface and C-filament growth in the sample interior after treatment in the humidified Ar – CH_4 atmosphere

case of D-series samples, despite substantial activity loss with time, C-nanofibers were never found, as already mentioned, and consequently no substrate cracking was noticed. The TEM investigation further revealed that during carbon filament growth Ni-grains suffered substantial elongation (Figure 9). The origin of catalyst reshaping is, according to the literature, correlated with the formation of the graphene layers at the grapheme-Ni interface [15].

The principle of the catalytic growth of filament-like carbon has been studied over a long period of time [32, 39-42]. It was explained by the following mechanism. The first step is the dissociative adsorption of methane gas on the Ni-surface. In this process, carbon atoms are deposited on the surface with the concomitant release of hydrogen. In the second step, carbon atoms dissolve and diffuse according to the bulk or surface mechanism through the Ni-pathway to the rear end, where the carbon atoms are incorporated into the new graphene layers of the growing nanofibers or graphitic plates. During carbon nanofibers growth the Ni-grains undergo changes of shape [15]. The thermodynamic driving force of this process is the formation of graphene out of carbon-containing gas. When this mechanism is adopted, sample cracking due to new filament growth becomes more consistent. The growing nanofibers push apart grains which are forming Ni-YSZ microstructures and thus increasing strain inside the Ni-YSZ framework, which is eventually the cause of crack formation. During the growth of C-fibers, Ni grains are often separated from the Ni-YSZ matrix (Figure 10).

While the physical degradation of the microstructure is the consequence of the growing cracks, catalyst activity change is more an indication to the Ni-surface poisoning due to the growing carbon layer. In view of the conducted methane dissociation tests together with the above-described C-filament growth, it is evident that dry methane conditions influence the catalyst activity far more then wet methane conditions. Specifically, in wet methane conditions only slight changes in catalyst activity toward methane dissociation were noticed. This fact implies that that Ni-surface coverage with new carbon (including carbon formation through methane dissociation and reaction of the new formed carbon with the

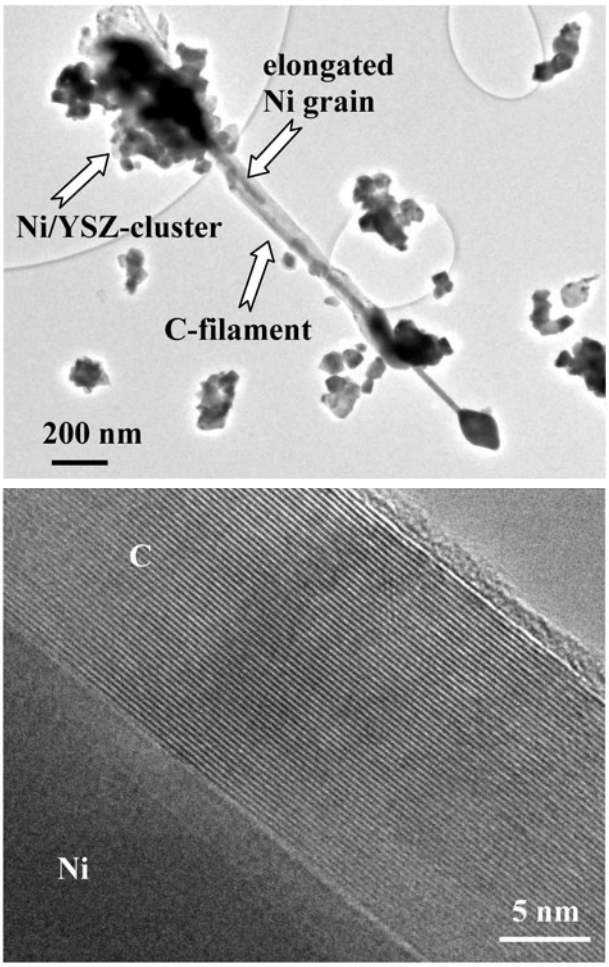

Figure 9. TEM image of Ni-YSZ cluster with denoted growing C-filament (left image) and higher magnification of the denoted part of C-filament revealing grapheme layers on elongated Ni-grain (right image)

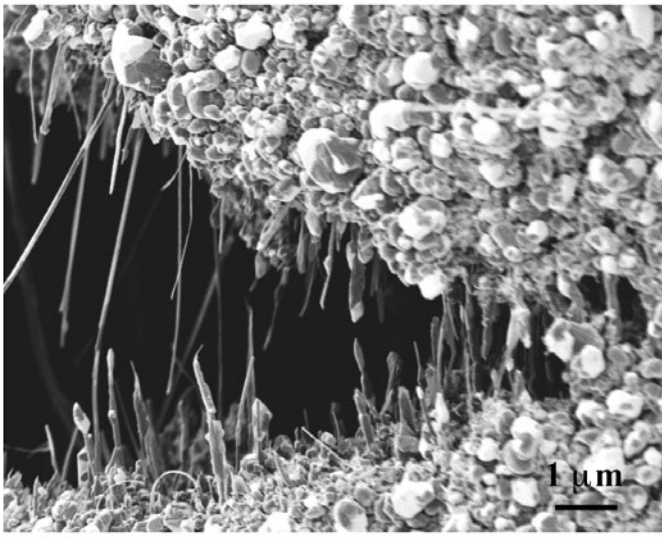

Figure 8. C-filament growth (sample B1) in the tip of the crack as a cause of the crack propagation (the crack developed perpendicular to the sample surface)

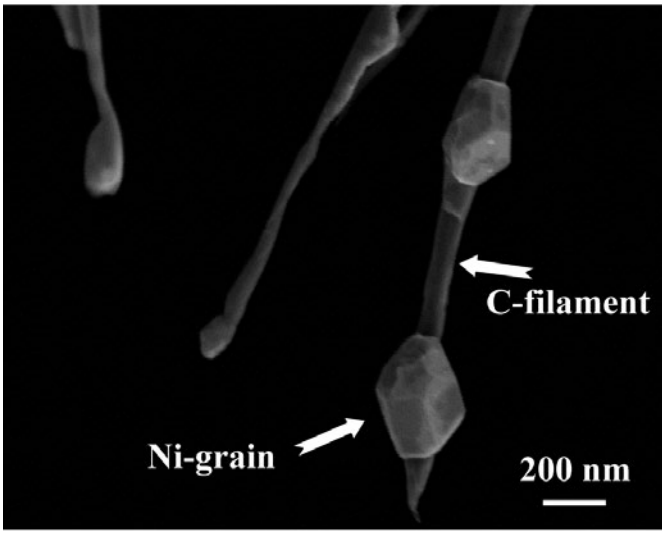

Figure 10. Separation of Ni-grains during C-filament growth in A'2 sample

surrounding atmosphere), carbon diffusion, and nanofibers growth must be highly balanced processes. Constant carbon mass gain in this case did not diminish hydrogen evolution, meaning that after isothermal conditions were reached, newly formed carbon either grew as filaments or increased thickness preformed graphite plates without poisoning the new Ni-surface. In contrast, in dry methane conditions dissociative methane adsorption is much faster then carbon incorporation into fibers or graphite plates and thus constantly poisons new Ni-surface. Eventually, the surface carbon structures are thick enough to prevent catalytic activity of the Ni-surface.

4. CONCLUSIONS

The main purpose of the paper was to illustrate the degradation process of Ni-YSZ cermets due to catalytic decomposition of CH_4 and subsequent carbon deposition. Carbon deposition on morphologically various Ni-YSZ substrates was studied in dry CH_4-Ar or humidified CH_4-Ar conditions.

The form of the deposited carbon differed significantly at the Ni-YSZ sample surface or catalyst interior. On the catalyst surface, Ni-grain encapsulation with the deposited carbon was noticed while carbon filaments grew inside the treated samples. The methane dissociation and carbon diffusion mechanism was adopted for C-filament growth. Carbon filament dimensions were very much influenced by the catalyst morphology and deposition conditions. The diameters of the grown filaments increased with the size of the Ni-grains; however, relatively large Ni-grains (0.98 μm) never promoted carbon-filament growth but rather encapsulation of Ni-grains with carbon plates. Carbon filaments also grew to larger diameters if the deposition temperature was higher.

Since carbon filaments always appeared inside formed cracks, C-fiber growth was proposed to be the cause for sample cracking and eventual complete physical degradation of the substrate microstructure. The change in catalyst activity, in contrast, was more an indication of the Ni poisoning due to the growing carbon layer on the catalyst surface. In dry methane conditions, dissociative methane adsorption overtakes the carbon diffusion and carbon filament or graphite growth while in wet-methane conditions with an S/C ratio of 0.82, the rates of all three processes are balanced. Consequently, catalytic activity of the Ni-YSZ composites in dry methane is reduced in time, while in wet methane conditions it remained nearly undiminished.

REFERENCES

1. S. Singhal, K. Kendall, High-temperature solid oxide fuel cells: fundamentals, design and applications, Elsevier Science Ltd., (2004)
2. M.C.J. Bradford, M.A. Vannice, CO_2 reforming of CH_4, Catal. Rev.-Sci. Eng., 41, 1, 1-42 (1999)
3. A.L. Lee, R.F. Zabransky, W.J. Huber, Internal reforming development for solid oxide fuel cells, Ind. Eng. Chem. Res., 29, 5, 766-773 (1990)
4. J.B. Wang, J.C. Jang, T.J. Huang, Study of Ni-samaria-doped ceria anode for direct oxidation of methane in solid oxide fuel cells, J. Power Sources, 122, 122-131 (2003)
5. Y. Lin, Z. Zhan, J. Liu, S.A. Barnet, Direct operation of solid oxide fuel cells with methane fuel, Solid State Ionics, 176, 1827-1835 (2005)
6. C.M. Finnerty, N.J. Coe, R.H. Cunningham, R.M. Ormerod, Carbon formation on and deactivation of nickel-based/zirconia anodes in solid oxide fuel cells running on methane, Catal. Today, 46, 2-3, 137-145 (1998)
7. R.M. Ormerod, Solid oxide fuel cells, Chem. Soc. Rev., 32, 17-28 (2003)
8. S. Park, J.M. Vohs, R.J. Gorte, Direct oxidation of hydrocarbons in a solid-oxide fuel cell, Nature (Lond.), 404, 265-267 (2000)
9. R.J. Gorte. S. Park, J.M. Vohs, C.H. Wang, Anodes for direct oxidation of dry hydrocarbons in a solid-oxide fuel cell, Adv. Mater., 12, 1465-1469 (2000)
10. E.S. Putna, J. Stubenrauch, J.M. Vohs, R.J. Gorte, Ceria-based anodes for the direct oxidation of methane in solid oxide fuel cells, Langmuir, 11, 12, 4832-4837 (1995)
11. O.A. Marina, C. Bagger, S. Primdahl. M. Mogensen, A solid oxide fuel cell with a gadolinia-doped ceria anode: preparation and performance, Solid State Ionics, 123, 199-208 (1999)
12. J.T.S. Irvine, A. Sauvet, Improved oxidation of hydrocarbons with new electrodes in high temperature fuel cells, Fuel Cells, 1, 205-210 (2001)
13. H.P. He, Y.Y. Huang, J.M. Vohs, R.J. Gorte, Characterization of YSZ–YST composites for SOFC anodes, Solid State Ionics, 175, 1-4, 171-176 (2004)
14. C. Mallon, K. Kendall, Sensitivity of nickel cermet anodes to reduction conditions, J. Power Sources, 145, 154-160 (2005)
15. E.P. Murray, T. Tsai, S.A. Barnett, A direct-methane solid oxide fuel cell with ceria-based anode, Nature, 400, 649-651 (1999)
16. T.V. Choudhary, D.W. Goodman, CO-free production of hydrogen via stepwise steam reforming of methane, J. Catal., 192, 2, 316-321 (2000)
17. C.H. Bartholomew, Mechanism of catalyst deactivation, Applied Catalysis A: General, 212, 17-60 (2001)
18. T. Osaki, T. Mori, Role of potassium in carbon-free CO_2 reforming of methane on K-promoted Ni/Al_2O_3 catalysts, J. Catal., 204, 1, 89-97 (2001)
19. H. Tu, U. Stimming, Advances, aging mechanisms and lifetime in solid-oxide fuel cells, Journal of Power Sources, 127, 284-293 (2004)
20. N. Laosiripojana, S. Assabumrungarat, Catalytic steam reforming of methane, methanol, and ethanol over Ni/YSZ: The possible use of these fuels in internal reforming SOFC, Journal of Power Sources, 163, 943-951 (2007)
21. A. Weber, B. Sauer, A.C. Muller, D. Herbstritt, E. Ivers-Tiffee, Oxidation of H_2, CO and methane in SOFC with Ni/YSZ-cermet anodes, Solid State Ionics, 152-153, 543-550 (2002)
22. C.E. Quincoces, S. Dicundo, A.M. Alvarez, M.G. Gonzales, Effect of addition of CaO on Ni/Al_2O_3 catalysts over CO_2 reforming of methane, Mater. Lett., 50, 21-27 (2001)
23. F. Frusteri, F. Arena, G. Calogero, T. Torre, A. Parmaliana, Potassium-enhanced stability of Ni/MgO catalysts in the dry-reforming of methane, Catal. Commun., 2, 2, 49-56 (2001)
24. H. He, J.M. Hill, Carbon deposition on Ni/YSZ composites exposed to humidified methane, Applied Catalysis, 317, 284-292 (2007)
25. T. Takeguchi, Y. Kani, T. Yano, R. Kikuchi, K. Eguchi, K. Tsujimoto, Y. Uchida, A. Ueno, K. Omoshiki, M. Aizawa, Study on steam reforming of CH_4 and C_2 hydrocarbons and carbon deposition on Ni-YSZ cermets, J. Power Sources, 112, 588-595 (2002)
26. T. Takeguchi, R. Kikuchi, T. Yano, K. Eguchi, K. Murata, Effect of precious metal addition to Ni-YSZ cermet on reforming of CH_4 and electrochemical activity as SOFC anode, Catalysis Today, 84, 217-222 (2003)
27. N.C. Triantafyllopoulos, S.G. Neophytides, The nature and binding strength of carbon adspecies formed during the equilibrium dissociative adsorption of CH_4 on Ni-YSZ cermet catalysts, Journal of Catalysis, 217, 324-333 (2003)
28. Fuel Cell Handbook, 5th ed., US Department of Energy, Morgantown, WV, (2000)
29. K. Sasaki, Y. Teraoka, Equilibria in fuel cell gases, J. Electrochem. Soc., 150, A878-A884 (2003)
30. I. Alstrup, B.S. Clausen, C. Olsen, R.H.H. Smits, J.R. Rostrup-Nielsen, Promotion of steam reforming catalysts, Stud. Surf. Sci. Catal., 119, 5-14 (1998)
31. W. Songtongkitcharoen, S. Assabumrungrat, V. Pavarajarn, N. Laosiripojana, P. Praserthdam, Comparison of carbon formation boundary in different modes of solid oxide fuel cells fueled by methane, Journal of Power sources, 142, 1-2, 75-80 (2005)
32. J. Rostrup-Nielsen, D.L. Trimm, Mechanisms of carbon formation on nickel-containing catalysts, J. Catal., 48, 1-3, 155-165 (1977)
33. Y. Zhang, K.J. Smith, Carbon formation thresholds and catalyst deactivation during CH_4 decomposition on supported Co and Ni catalysts, Catalysis Letters, 95, 7-12 (2004)
34. M. Marinšek, K. Zupan, J. Maček, Citrate-nitrate gel transformation behavior during the synthesis of combustion-derived NiO-yttria-stabilized zirconia composite. J. mater. res., 18, 7, 1551-1560 (2003)
35. M. Marinšek, J. Padežnik-Gomilšek, I. Arčon, M. Čeh, A. Kodre, J. Maček, Structure development of NiO-YSZ oxide mixtures in simulated citrate-nitrate combustion synthesis. J. Am. Ceram. Soc., 90, 10, 3274-3281 (2007)
36. Y. Ando, X. Zhao, T. Sugai, M. Kun, Growing carbon nanotubes, Materials Today, 7, 22-29 (2004)
37. M.L. Toebes, J.H. Bitter, A. Jos van Dillen, K.P. de Jong, Impact of the structure and reactivity of nickel particles on the catalytic growth of carbon nanofibers, Catalysis Today, 76, 33-42 (2002)
38. N.M. Rodriguez, A. Chambers, R.T.K. Baker, Catalytic engineering of carbon nanostructures, Langmuir, 11, 3862-3866 (1995)
39. K.P. de Jong, J.W. Geus, Carbon nanofibers - catalytic synthesis and applications, Catal. Rev.-Sci. Eng., 42, 481-510 (2000)
40. F. Abild-Pedersen, J.K. Nørskov, J.R. Rostrup-Nielsen, J. Sehested, S. Helveg, Mechanism of catalytic nanofiber growth studied by *ab initio* density functional theory calculations, Physical Review B, 73, 115419-1 – 115419-13 (2006)
41. C. Klinke, J.M. Bonard, K. Kern, Thermodynamic calculations on the catalytic growth of multiwall carbon nanotubes, Physical Review B, 71, 035403-1 – 035403-7 (2005)
42. R.T.K. Baker, Catalytic growth of carbon filaments, Carbon, 27, 315-323 (1989)

Recibido: 15/6/2010
Aceptado: 24/5/2011